
This item was submitted to [Loughborough's Research Repository](#) by the author.
Items in Figshare are protected by copyright, with all rights reserved, unless otherwise indicated.

Geometrically non-linear analysis of composite laminated plates subjected to low-velocity impact

PLEASE CITE THE PUBLISHED VERSION

<http://article.sapub.org/10.5923.s.cmaterials.201310.04.html>

PUBLISHER

© Scientific & Academic Publishing

VERSION

AM (Accepted Manuscript)

PUBLISHER STATEMENT

This work is made available according to the conditions of the Creative Commons Attribution-NonCommercial-NoDerivatives 4.0 International (CC BY-NC-ND 4.0) licence. Full details of this licence are available at: <https://creativecommons.org/licenses/by-nc-nd/4.0/>

LICENCE

CC BY-NC-ND 4.0

REPOSITORY RECORD

Wang, Simon, Xiuqin Zhang, Yingshun Zhang, and Chenyu Zhang. 2014. "Geometrically Non-linear Analysis of Composite Laminated Plates Subjected to Low-velocity Impact". figshare. <https://hdl.handle.net/2134/16235>.

Geometrically Non-linear Analysis of **Laminated Composite Plates** Subjected to Low-Velocity Impact

Simon Wang^{3*}, Xiuqin Zhang¹, Yingshun Zhang², Chenyu Zhang³

¹ Taiyuan University of Technology, 79 West Yingze Street, Taiyuan 030024, Shanxi, China

² Doosan Babcock Energy Limited, Porterfield Road, Renfrew PA4 8DJ, UK

^{3,3*} Department of Aeronautical and Automotive Engineering, Loughborough University, Loughborough LE11 3TU, UK

ABSTRACT: A B-spline finite strip model is developed in the context of a layer-wise plate theory for analysing the geometrically non-linear transient response of laminated composite plates subjected to transverse low-velocity impact. To simplify the complicated contact analysis, a Hertz-type contact law has been incorporated into the finite strip (FS) model for accounting for the contact behaviour. The model includes the geometrical non-linearity through use of von Karman's non-linear strain-displacement relationship. The resulting non-linear dynamic problem is solved using the Newmark time-stepping scheme together with Newton-Raphson iteration. Several numerical applications are described and a close comparison is found between the results calculated through the present model and the existing analytical and experimental results.

Keywords: Laminated Composite, Low-velocity Impact, Geometrical non-linearity, Transient, B-spline Finite Strip

1 Introduction

Laminated composite structures have played an important role in aircraft, vehicles and many other demanding applications because of their high strength-to-weight and high stiffness-to-weight ratios. As it is well known, however, these structures are very susceptible to low-velocity impact damage, which can be introduced during manufacture and in service. Impact induced damage can have a significant effect on the strength, stability and reliability of the structures. Therefore, great concern has been received on the low-velocity impact of the structures [1]. For understanding low-velocity impact response of composite structures, several analytical approaches have been used by a number of researchers. These approaches vary from simple mathematical models, such as spring-mass models and energy-balance models, to more complicated dynamic analysis of the impact events.

In spring-mass models, the structure is represented by an assemblage of springs and masses. The low-velocity impact event is simulated by a discrete system with a few degrees of freedom. These kinds of model are generally used to estimate the impact force history for the impact events in which the structures behave quasi-statically. Caprino et al [2] used a single degree of freedom model to predict elastic impact response of a small glass cloth-polyester panel due to a drop weight impact. In their model, the panel is represented as a linear spring of stiffness k , which corresponds to the static rigidity of the panel at the impact point. Similar models are also used by others [3,4,5]. Shivakumar et al [6] suggested a two degree of freedom model, in which the impactor and the plate are treated as two masses, and four springs are used to represent the contact stiffness and the bending, shear and membrane rigidities of the plate. Bucinell et al [7] employed the same model to study the response of composite plates to impacts. In the two degree of freedom model of Sjoblom et al [8], the plate and contact rigidity is modelled separately using two springs. Toh et al [9,10] also used a two-degree of freedom model to predict the impact force. Gong and Lam [11] proposed an improved two degree of freedom spring-mass model by implementing the structural damping to determine the contact force between the target and striker during impact. Another kind of frequently used simple models for the impact events in which the structures behave quasi-statically are energy-balance models [6,12]. In these models, it is assumed that the velocity of the impactor becomes zero when the structure reaches its maximum deflection. Energy-balance models allow direct estimate of the maximum contact force, considering the conservation of energy without having to compute the entire time history. Whilst they are useful in understanding the main features of low-velocity impact events, the above-mentioned simple models are inadequate in accounting for the dynamic nature of the composite structures under low-velocity impact. For understanding the initiation and propagation of the low-velocity impact damage as well as the interaction between the damage and plate dynamic response, dynamic analysis is often needed for accurate prediction of low-velocity impact behaviour of the composite laminates. In addition, it is the case that for many situations the responses of the structures in low-velocity impact events cannot be viewed as quasi-static ones. Therefore, it is very important to have an insight into dynamic response of the impacted structures.

Dynamic analysis of low-velocity impact response of laminated composites generally involves the global dynamic response of the laminates and the local contact between the impactor and the structure. To model the contact, one of the possibilities is based on a formulation of the joint contact problem for the system of impactor-target. This is tightly connected with the particular numerical method to be applied, for instance, finite element method, finite difference method, or other method based on some variational principles. In FEM analysis of the impact contact problem, contact elements are used to model the laminate and the impactor

[13,14,15,16,17,18,19]. The solution of the contact problem may be achieved using several contact algorithms such as the Lagrange multiplier method [13] and the penalty method [19]. The Lagrange multiplier method has the advantage of enforcing the exact constraints, but induces additional parameters which substantially enlarge the overall size of the equations to be solved. The penalty method is relatively simple and does not require additional equations. With contact algorithms, the contact state is detected at each time step and the contact constraints are imposed to the contacting nodes/elements once contact occurs. Since contact is a non-linear problem, full analysis of the impact contact for the system of impactor-target is a complex and time-consuming procedure. Hence, simplification of the contact problem is often made through use of the contact laws in impact analysis of composite laminates. Yang and Sun [20] have proposed a contact law for contact between a sphere and a composite laminate based on static indentation tests. This contact law accounts for permanent indentation after unloading cycles and uses different relationships between the contact force and the indentation for loading, unloading and reloading processes. Tan and Sun [21] further studied the unloading and reloading process and proposed a modified version of the contact law. Experimental observations [22,23] confirm that loading rate effects during low-velocity impact of composites are insignificant. This suggests that statically determined contact laws may be used for impact analysis of composite structures. The above-mentioned contact laws developed by Sun and his co-workers have gained extensive use in analysing the dynamic response of composite laminates to impact. It should be noted that these contact laws do not give the contact stress distribution under the indenter. Determination of the contact stress distribution has to appeal to analytical method. In addition, these contact laws have not accounted for damage effect on force-indentation relationship. Wu and Shyu [24] showed that the contact phenomenon is different in small and large indentation stages due to occurrence of laminate damage. In the small indentation stage where the plate is intact, the change of laminate stacking sequence has an insignificant effect on the force-indentation relationship. Beyond the small indentation stage, damage occurs and the indentation spring is stiffened as a result of matrix crack and delamination damage of the laminates. The contact behaviour during low-velocity impact is very similar to that in a static test.

Because of the complexity of the impact problem, closed-form exact solutions exist only for simple cases. In most situations, approximate analytical and/or numerical methods have to be adopted. In conjunction with contact laws, dynamic analyses of low-velocity impact of composite laminates have been carried out analytically by a number of researchers. Sun and Chattopadhyay [25] studied a simply-supported orthotropic plate subjected to central impact using **first-order shear deformable plate theory (FSDPT)** developed by

Whitney and Pagano [26]. Dobyns [27] used the same method but replaced the concentrated impact load by a uniform patch pressure to avoid transverse shear force singularity at the contact point. Qian and Swanson [28] examined two solution techniques which were based on series expansion. One of them was based on a Rayleigh-Ritz approach with numerical integration in time, and the other was an analytical approach using Laplace transformation of the governing differential equations, but requiring a linearisation of the contact law. Carvalho and Soares [29] studied a simply-supported composite plate subjected to an impact load utilising the technique of Fourier series expansion for the solution of the dynamic plate equations. Comparison was made between the numerical solution technique based on Newmark integration method and the analytical formulation using the Laplace transform technique. Pierson and Vaziri [30] presented a Fourier series solution that retains the frequencies associated with rotary inertia effects. A double Fourier series expansion and the Timoshenko small-increment method were used by Ambur et al [31,32] for determining the transient response of simply supported, rectangular laminated plates subjected to impact loads. Heitzer [33] studied the interaction of an impactor and a clamped, anisotropic plate at low-velocities by assuming a series expansion for the plate deflection. Large deflection was taken into account and the contact law was used.

It is well known that FEM is one of the most powerful tools of solution in structural analysis. Besides 2D or 3D finite element analyses of the joint impactor-target system [13,14,15,16,17,18,19,34,35,36], many researchers have employed the FEM in conjunction with contact laws for the analyses of composite laminates due to low-velocity impact. Sun and his collaborators [21,37,38] used static indentation laws and FEM based on FSDPT to analyse the impact responses of composite laminates. The initially stressed composite laminates were studied in [37] and dynamic large deflection was considered in [38]. Wu and Chang [39] developed a 3D finite element code for transient dynamic analysis of laminated composite plates due to transverse foreign object impact in which a contact law is incorporated. Combined with failure criteria this 3D finite element code has been used by Wu and Springer [40], Choi and Chang [41], Finn and Springer [42,43], and Scarponi et al [44] for failure analyses of impacted laminates. Choi and Chang [45,46,47] developed a 2D FEM for studying the impact damage of laminated composite beam resulting from the line-loading impact. Davies and Zhang et al [48,49,50,51] investigated impact-induced damage using FEM based on Mindlin's plate theory combined with a contact law [22]. The FEM based on FSDPT and a Hertzian-type indentation law was employed by Hu et al [36] for analysing the transient response of composite laminates with multiple delaminations subjected to low-velocity impact.

It appears that the majority of previous analytical and numerical analyses are limited to small-deflection behaviour. Although such linear analyses are practical and useful for many impact problems of composite structures, it is often the case that the geometric non-linearity (GNL) has very significant effects on the impact response.

In this paper, a layer-wise B-spline finite strip model developed in [52] is extended through introduction of time dimension for the GNL transient analysis of laminated composite plates subjected to transverse low-velocity impact of spherical object within the context of a layer-wise plate theory [53]. It is noted that in References [54,55] a B-spline FSM has been used for transient analysis of laminated composite plates subjected to dynamic loads based on FSDPT. In the present study, the geometrical non-linearity is taken into consideration by use of von Karman's non-linear strain-displacement relationship. The dynamic problem is solved using the Newmark time-stepping scheme in the time domain and the solution of the resulting non-linear equations is sought with Newton-Raphson iteration. The impact problem in the small-deflection regime is briefly discussed as well. Several numerical applications are presented. It is noted that material damage and delamination are not dealt with in the current work.

2 Problem description and fundamentals

Consider a laminated rectangular plate with arbitrary lay-ups subjected to transverse low-velocity impact of a spherical object as shown in Fig. 1. The impactor is of radius r_s , mass m and initial velocity v_0 . It is assumed that the vibrations of the elastic impactor can be neglected. An orthogonal Cartesian co-ordinate system x_i ($i=1,2,3$) is used in this paper.

2.1 Basic Plate Equations

In the present study, the layer-wise plate theory proposed by Reddy [53] is adopted for representation of displacement behaviour in the plate. Through the thickness direction, the laminated plate is divided into a desired number, N , of numerical layers, which can be less than, equal to, or greater than the number of physical

layers. The assumed displacements (\bar{u}_α , \bar{u}_3) at a general point of the laminate, with t as the time dimension, take the form as what follows.

$$\begin{aligned}\bar{u}_\alpha(x_\beta, x_3, t) &= u_\alpha(x_\beta, t) + \Psi^i(x_3)u_\alpha^i(x_\beta, t) \\ \bar{u}_3(x_\beta, x_3, t) &= u_3(x_\beta, t)\end{aligned}\quad (1)$$

Where the usual Cartesian indicial notation is adopted. The Greek subscripts, which take values 1 and 2, and subscript 3 refer to x_1 , x_2 , x_3 directions, respectively. Repeated indices imply the summation convention. Superscript i , ranged from 1 to N , is related to the nodes through the thickness. u_α and u_3 denote the three displacement components of the reference plane ($x_3=0$). Ψ^i are piecewise continuous functions and defined as

$$\Psi^i = R_{ik} \tilde{\Psi}^k \quad (2)$$

where i is ranged from 1 to N and \tilde{k} from 1 to $N+1$. $\tilde{\Psi}^k$ is defined in terms of linear Lagrange interpolation functions

$$\Psi^{\tilde{k}}(x_3) = \begin{cases} \frac{x_3 - x_3^{\tilde{k}-1}}{x_3^{\tilde{k}} - x_3^{\tilde{k}-1}} & x_3 \in [x_3^{\tilde{k}-1}, x_3^{\tilde{k}}] \in [x_3^1, x_3^{N+1}] \\ \frac{x_3^{\tilde{k}+1} - x_3}{x_3^{\tilde{k}+1} - x_3^{\tilde{k}}} & x_3 \in [x_3^{\tilde{k}}, x_3^{\tilde{k}+1}] \in [x_3^1, x_3^{N+1}] \\ 0 & x_3 \notin [x_3^1, x_3^{N+1}] \end{cases} \quad (3)$$

and R_{ik} is defined as

$$R_{ik} = \begin{cases} 1 & i = \tilde{k} < m \quad \text{or} \quad i = \tilde{k} - 1 \geq m \\ x_3^m / x_3^{m+1} & i = \tilde{k} = m \\ 0 & \text{others} \end{cases} \quad (4)$$

Here m is the number of the layer at which the reference plane is.

The resulting displacement configuration is shown in Fig.2.

The expressions of the strain-displacement relationship can be given by substitution of the displacement field Eq.1 in the Green's expressions for in-plane non-linear strains and neglecting higher order terms in a manner consistent with von Karman's assumptions. They are:

$$\begin{aligned}\bar{\varepsilon}_{\alpha\beta} &= \varepsilon_{\alpha\beta} + \Psi^i \varepsilon_{\alpha\beta}^i \\ \bar{\gamma}_{\alpha 3} &= \gamma_{\alpha 3} + \Psi_{,3}^i \gamma_{\alpha 3}^i\end{aligned}\quad (5)$$

where

$$\begin{aligned}
\varepsilon_{\alpha\beta} &= \frac{1}{2}(u_{\alpha,\beta} + u_{\beta,\alpha}) + \frac{1}{2}u_{3,\alpha}u_{3,\beta} \\
\varepsilon_{\alpha\beta}^i &= \frac{1}{2}(u_{\alpha,\beta}^i + u_{\beta,\alpha}^i) \\
\gamma_{\alpha 3} &= u_{3,\alpha} \quad \gamma_{\alpha 3}^i = u_{\alpha}^i
\end{aligned} \tag{6}$$

The strain energy of the laminate considered can be obtained as an integral over the reference plane area S. The result is:

$$U = \frac{1}{2} \iint_S (N_{\alpha\beta} \varepsilon_{\alpha\beta} + N_{\alpha\beta}^i \varepsilon_{\alpha\beta}^i + Q_{\alpha 3} \gamma_{\alpha 3} + Q_{\alpha 3}^i \gamma_{\alpha 3}^i) dx_1 dx_2 \tag{7}$$

where

$$\begin{Bmatrix} N_{\alpha\beta} \\ N_{\alpha\beta}^i \end{Bmatrix} = \begin{bmatrix} A_{\alpha\beta\gamma\omega} & B_{\alpha\beta\gamma\omega}^k \\ B_{\alpha\beta\gamma\omega}^i & D_{\alpha\beta\gamma\omega}^{ik} \end{bmatrix} \begin{Bmatrix} \varepsilon_{\gamma\omega} \\ \varepsilon_{\gamma\omega}^k \end{Bmatrix} \quad \begin{Bmatrix} Q_{\alpha 3} \\ Q_{\alpha 3}^i \end{Bmatrix} = \begin{bmatrix} A_{\alpha 3\beta 3} & B_{\alpha 3\beta 3}^k \\ B_{\alpha 3\beta 3}^i & D_{\alpha 3\beta 3}^{ik} \end{bmatrix} \begin{Bmatrix} \gamma_{\beta 3} \\ \gamma_{\beta 3}^k \end{Bmatrix} \tag{8}$$

$N_{\alpha\beta}$, $N_{\alpha\beta}^i$, $Q_{\alpha 3}$, and $Q_{\alpha 3}^i$ are generalised stresses per unit length. $A_{\alpha\beta\gamma\omega}$, $B_{\alpha\beta\gamma\omega}^i$, etc, are the stiffness coefficients of the laminate which are defined as

$$\begin{aligned}
(A_{\alpha\beta\gamma\omega}, B_{\alpha\beta\gamma\omega}^i, D_{\alpha\beta\gamma\omega}^{ik}) &= \int_{-h/2}^{h/2} Q_{\alpha\beta\gamma\omega} (1, \Psi^i, \Psi^i \Psi^k) dx_3 \\
(A_{\alpha 3\beta 3}, B_{\alpha 3\beta 3}^i, D_{\alpha 3\beta 3}^{ik}) &= \int_{-h/2}^{h/2} Q_{\alpha 3\beta 3} (1, \Psi_{,3}^i, \Psi_{,3}^i \Psi_{,3}^k) dx_3
\end{aligned} \tag{9}$$

where $Q_{\alpha\beta\gamma\omega}$ and $Q_{\alpha 3\beta 3}$ denote the transformed reduced stiffness coefficients. $Q_{\alpha\beta\gamma\omega}$ possess symmetry in the indices α and β , γ and ω , and the pairs of $\alpha\beta$ and $\gamma\omega$. The similar symmetrical property also applies to $Q_{\alpha 3\beta 3}$.

2.2 Finite strip approximation

The whole plate is modelled with a number of finite strips along the crosswise x_2 -direction. Each strip is further partitioned longitudinally into q sections. A typical individual finite strip element (quadratic strip) is shown in Fig.3. Over the strip each of the fundamental displacement quantities u_α , u_3 , and u_α^i can be approximated as a function of multiplicative type, in which $q+k$ B-spline functions of degree k are used in the longitudinal x_1 -direction and simple polynomials of degree n in the crosswise x_2 -direction. Mathematically, the fundamental displacement quantities are given as

$$\begin{Bmatrix} u_\alpha \\ u_3 \\ u_1^i \\ u_2^i \end{Bmatrix} = N^I \begin{bmatrix} \Phi & & & \\ & \Phi & & \\ & & \Phi_{-1} & \\ & & & \Phi \end{bmatrix} \begin{Bmatrix} \mathbf{d}_\alpha^I \\ \mathbf{d}_3^I \\ \mathbf{d}_1^i \\ \mathbf{d}_2^i \end{Bmatrix} \tag{10}$$

Here \mathbf{d}_α , \mathbf{d}_3 and \mathbf{d}_α^i are column matrices of generalised displacement parameters associated with u_α, u_3 and u_α^i , respectively. The row matrices Φ and Φ_{-1} are modified B-spline function bases of order k and $k-1$ in the longitudinal x_1 -direction. N^l are polynomial functions of degree n in the crosswise x_2 -direction and here Lagrangian shape functions are used. The superscript i , ranged from 1 to N , is related to the nodes through the thickness. The capital superscript l , ranging from 0 to n , denotes the number of a reference line in the crosswise x_2 -direction of the strip.

3 Governing equations of motion

In the absence of damping, the governing equations of the plate motion can be given through use of Hamilton's principle in terms of strain energy U , kinetic energy T and potential energy W as

$$\mathbf{M}\ddot{\mathbf{d}} + \mathbf{K}\mathbf{d} = F\mathbf{c} + \mathbf{f} \quad (11)$$

where \mathbf{M} and \mathbf{K} denote the mass matrix and the effective stiffness matrix, respectively, and \mathbf{K} are functions of \mathbf{d} . \mathbf{d} and \mathbf{f} are column matrices of generalised displacement parameters and generalised force due to applied loading. F is impact contact force. \mathbf{c} is a column matrix, resulting from the product of the polynomials in the x_2 -direction and the B-spline functions in the x_1 -direction at the impacting point of the plate, and $\mathbf{c}^T\mathbf{d}$ defines the deflection of the reference plane of the plate at impact point.

The relationship between the contact force F and the indentation depth α is assumed as [20]

$$F = k_c \alpha^{3/2} \quad \text{when loading} \quad (12a)$$

$$F = F_m [(\alpha - \alpha_0) / (\alpha_m - \alpha_0)]^{5/2} \quad \text{when unloading} \quad (12b)$$

$$F = F_m [(\alpha - \alpha_0) / (\alpha_m - \alpha_0)]^{3/2} \quad \text{when reloading} \quad (12c)$$

where k_c is a constant. F_m denotes the maximum contact force just before unloading, α_m is the indentation corresponding to F_m , and α_0 is the permanent indentation during the loading/unloading cycle. k_c can be determined by experiment or simply calculated from the modified Hertz contact coefficient proposed by Sun [20] as

$$k_c = \frac{4}{3} \sqrt{r_s} [(1 - \nu_s^2) / E_s + 1 / E_2]^{-1} \quad (13)$$

here r_s , ν_s and E_s are the radius, the Poisson's ratio and the Young's modulus of the impactor, respectively, and E_2 is the transverse modulus of elasticity of the plate.

Eq.12 can be expressed in a general form as

$$F = k_s (\alpha - \alpha_0)^q \quad (14)$$

where k_s and q are the contact coefficient and a constant, respectively. It is noticed that for the loading, unloading and reloading process α_0 , k_s and q may be different.

The indentation depth α is the difference of the displacement of the impactor and the deflection of the reference plane of the plate at impact point, so that

$$(F / k_s)^{1/q} + \alpha_0 = v_0 t - \frac{1}{m} s - \mathbf{c}^T \mathbf{d} \quad (= \alpha) \quad (15)$$

where

$$s = \int_0^t \int_0^t F dt dt \quad (16)$$

Eqs.11 and 15 together with appropriate initial conditions define the present impact dynamic problem. It is here assumed that \mathbf{d} , $\dot{\mathbf{d}}$ and $\ddot{\mathbf{d}}$ are known at time $t = 0$ and F , s , \dot{s} are equal to zero at time $t = 0$.

4 Problem solution

In the time domain the impact problem defined in Eqs.11 and 15 can be solved with a few of different approaches. In the present investigation the solution of the problem is sought using the popular Newmark time integral algorithm. Suppose that the time period concerned is divided into a number of equal time intervals Δt and consider the satisfaction of Eqs.11 and 15 at time $(n+1)\Delta t$ and write

$$\mathbf{M} \ddot{\mathbf{d}}_{n+1} + \mathbf{K} \mathbf{d}_{n+1} = F_{n+1} \mathbf{c} + \mathbf{f}_{n+1} \quad (17a)$$

$$(F_{n+1} / k_s)^{1/q} + \alpha_0 = v_0 (n+1)\Delta t - \frac{1}{m} s_{n+1} - \mathbf{c}^T \mathbf{d}_{n+1} \quad (17b)$$

with approximations for \mathbf{d}_{n+1} , $\dot{\mathbf{d}}_{n+1}$, s_{n+1} and \dot{s}_{n+1} as

$$\mathbf{d}_{n+1} = \mathbf{d}_n + \Delta t \dot{\mathbf{d}}_n + \frac{\Delta t^2}{2} (1 - \beta_2) \ddot{\mathbf{d}}_n + \frac{\Delta t^2}{2} \beta_2 \ddot{\mathbf{d}}_{n+1} \quad (18a)$$

$$\dot{\mathbf{d}}_{n+1} = \dot{\mathbf{d}}_n + \Delta t (1 - \beta_1) \ddot{\mathbf{d}}_n + \Delta t \beta_1 \ddot{\mathbf{d}}_{n+1}$$

$$\begin{aligned}
s_{n+1} &= s_n + \Delta t \dot{s}_n + \frac{\Delta t^2}{2} (1 - \beta_2) F_n + \frac{\Delta t^2}{2} \beta_2 F_{n+1} \\
\dot{s}_{n+1} &= \dot{s}_n + \Delta t (1 - \beta_1) F_n + \Delta t \beta_1 F_{n+1}
\end{aligned} \tag{18b}$$

where the parameters β_1 and β_2 can be chosen as such that good approximation properties to the algorithm are yielded. In this study the constant-average-acceleration version of Newmark method is used, and consequently, $\beta_1 = \beta_2 = 1/2$. The algorithms yield unconditional stability for linear problems at least. Belytschko and Schoeberle [56] use the Newmark- β method for a nonlinear structural dynamics problem. Their proof of unconditional stability with $\beta = 0.25$ using an energy method applies only to nonlinear material properties but they state that numerical results show unconditional stability with geometric nonlinearity also.

Substitution of Eq.18 into Eq.17 leads to a set of non-linear equations in which the unknowns are $\ddot{\mathbf{d}}_{n+1}$ and F_{n+1} . The non-linear equations can be written in terms of residual forces as

$$\mathbf{R} = \mathbf{M} \ddot{\mathbf{d}}_{n+1} + \mathbf{K} (\mathbf{d}_n + \Delta t \dot{\mathbf{d}}_n + \frac{\Delta t^2}{2} (1 - \beta_2) \ddot{\mathbf{d}}_n + \frac{\Delta t^2}{2} \beta_2 \ddot{\mathbf{d}}_{n+1}) - F_{n+1} \mathbf{c} - \mathbf{f}_{n+1} = \mathbf{0} \tag{19a}$$

$$r = \mathbf{c}^T \mathbf{d}_{n+1} + (F_{n+1} / k_s)^{1/q} + \frac{1}{m} (s_n + \Delta t \dot{s}_n + \frac{\Delta t^2}{2} (1 - \beta_2) F_n + \frac{\Delta t^2}{2} \beta_2 F_{n+1}) + \alpha_0 - v_0 (n+1) \Delta t = 0 \tag{19b}$$

To seek the solution of the non-linear problem defined in Eq.19, the Newton-Raphson iteration scheme is here adopted. It is noted that, to the first order, Eq.19 can be approximated as

$$\mathbf{R}^{i+1} \approx \mathbf{R}^i + (\mathbf{M} + \frac{\Delta t^2}{2} \beta_2 \mathbf{K}_T^i) \delta \ddot{\mathbf{d}}_{n+1}^i - \delta F_{n+1}^i \mathbf{c} = \mathbf{0} \tag{20a}$$

$$r^{i+1} \approx r^i + \frac{\Delta t^2}{2} \beta_2 \mathbf{c}^T \delta \ddot{\mathbf{d}}_{n+1}^i + k_t \delta F_{n+1}^i = 0 \tag{20b}$$

where

$$\mathbf{K}_T^i = \left. \frac{\partial (\mathbf{K} \mathbf{d}_{n+1})}{\partial \mathbf{d}_{n+1}} \right|_{\mathbf{d}_{n+1} = \mathbf{d}_{n+1}^i} \tag{21}$$

$$k_t^i = \frac{(F_{n+1}^i)^{1/q-1}}{q k_s^{1/q}} + \frac{1}{m} \frac{\Delta t^2}{2} \beta_2$$

$$\delta \ddot{\mathbf{d}}_{n+1}^i = \ddot{\mathbf{d}}_{n+1}^{i+1} - \ddot{\mathbf{d}}_{n+1}^i \quad \delta F_{n+1}^i = F_{n+1}^{i+1} - F_{n+1}^i \tag{22}$$

Here superscript i denotes the iteration counter. \mathbf{K}_T^i is the symmetric tangent stiffness matrix evaluated at iteration i . k_t^i is defined with the condition of $F_{n+1}^i > 0$. $\delta\ddot{\mathbf{d}}_{n+1}^i$ and δF_{n+1}^i are increments, or iterative corrections, of the unknowns $\ddot{\mathbf{d}}_{n+1}$ and F_{n+1} at iteration i , respectively, and they can be given from Eq.20 as

$$\begin{aligned}\delta\ddot{\mathbf{d}}_{n+1}^i &= -\left(\mathbf{M} + \frac{\Delta t^2}{2}\beta_2\mathbf{K}_T^i + \frac{1}{k_t^i}\frac{\Delta t^2}{2}\beta_2\mathbf{c}\mathbf{c}^T\right)^{-1}\left(\mathbf{R}^i + \frac{r^i}{k_t^i}\mathbf{c}\right) \\ \delta F_{n+1}^i &= -\frac{1}{k_t^i}\left(r^i + \frac{\Delta t^2}{2}\beta_2\mathbf{c}^T\delta\ddot{\mathbf{d}}_{n+1}^i\right)\end{aligned}\quad (23)$$

Through the use of Eq.22 with the corrections given in Eq.23, the iteration procedure results in improved solution for the unknowns $\ddot{\mathbf{d}}_{n+1}$ and F_{n+1} . The procedure is repeated until the following convergence criteria are satisfied

$$\sqrt{\frac{\delta\mathbf{d}_{n+1}^i{}^T\delta\mathbf{d}_{n+1}^i}{\mathbf{d}_{n+1}^i{}^T\mathbf{d}_{n+1}^i}} < \varepsilon \quad \text{and} \quad \left|\frac{\delta F_{n+1}^i}{F_{n+1}^i}\right| < \varepsilon \quad (24)$$

where $\varepsilon = 0.0005$ is used in this work.

Up to now the impact dynamic transients are concerned with geometric non-linearity and the solution procedure is described in details as above. For comparison, the impact problem is also investigated within the context of small deflection in this paper. In fact there exists no difference between the geometric non-linear and linear analyses of the impact problem in the temporal approximation. Within a time step, however, the solution procedure used for the linear transient response is different from that described above for the non-linear one, and is here discussed below.

In the case of geometric linear analyses of the impact problem, the non-linear strain terms are ignored in the strain-displacement relationship. As a result, the stiffness matrix \mathbf{K} becomes independent of the plate displacement. From Eq.19a the following equations can be given

$$\left(\mathbf{M} + \frac{\Delta t^2}{2}\beta_2\mathbf{K}\right)(\ddot{\mathbf{d}}_{n+1}^c, \ddot{\mathbf{d}}_{n+1}^f) = (\mathbf{c}, \mathbf{f}_{n+1} - \mathbf{K}(\mathbf{d}_n + \Delta t\dot{\mathbf{d}}_n + \frac{\Delta t^2}{2}(1-\beta_2)\ddot{\mathbf{d}}_n)) \quad (25)$$

and

$$\ddot{\mathbf{d}}_{n+1} = F_{n+1}\ddot{\mathbf{d}}_{n+1}^c + \ddot{\mathbf{d}}_{n+1}^f \quad (26)$$

Eqs.25 and 26 together with Eq.19b define the present impact problem in terms of small deflection. It is obvious that Eq.25 defines two sets of linear algebraic equations with respect to unknowns $\ddot{\mathbf{d}}_{n+1}^c$ and $\ddot{\mathbf{d}}_{n+1}^f$.

These two sets of linear equations can be solved simultaneously since they share the same coefficient matrix. The solution procedures involve triangular decomposition of the coefficient matrix and then forward elimination and back substitution. Most of the computing efforts are expended in the procedure of triangular decomposition of the coefficient matrix during the solution of the equations. Noting the coefficient matrix is independent of time increments, the triangular decomposition of the coefficient matrix is performed ahead of the time iteration in the present methodology and in each time increment only the forward elimination and back substitution are involved. With this strategy, the computer efforts can be greatly reduced.

Substitution of Eq.26 into Eq.19b leads to a non-linear equation with respect to F_{n+1} , and again, the Newton-Raphson iteration technique is adopted for the solution of the non-linear equation. The iterative corrections for F_{n+1} can be written as

$$\delta F_{n+1}^i = -\frac{r^i}{k_t^i + \mathbf{c}^T \mathbf{d}_{n+1}^c} \quad (27)$$

where k_t^i and r^i are the same as those given before and \mathbf{d}_{n+1}^c are evaluated from Eq.19.

5 Numerical applications

The above analysis procedure has been implemented in an in-house computer software. It can be used for impact problems and, neglecting impact-related terms, for plate transient response under dynamic loading. Numerical tests have been conducted to verify the validity of the present computational model, which include a series of examples of composite laminate plates under low-velocity impact. The selected examples of the impact problem refer to two typical kinds of low-velocity impact events, i.e. small impact mass with relatively high speed and large mass with low speed. In all the applications, the quadratic Lagrangian shape functions are applied in the crosswise x_2 -direction. Unless otherwise specified, the simply supported boundary conditions are defined such that the plate is simply supported for out-of-plane behaviour whilst the in-plane movement of the sides is constrained in the tangent direction but allowed in the normal direction. For the impact problems considered, the contact law defined in Eq.12a is used for both the loading and unloading processes. The details are presented in the following subsections.

5.1 Impact of a [0/90/0/90/0]_s plate

Consider the impact problem involving central impact of a simply supported square T300/934 graphite/epoxy [0/90/0/90/0]_s plate by a steel object with a spherical impact tip of diameter 12.7mm. The plate has dimension 200 × 200 × 2.69 mm. The material properties of a T300/934 graphite/epoxy lamina are given as

$$E_1 = 120 \text{ GPa}, E_2 = 7.9 \text{ GPa}, \nu_{12} = 0.3$$

$$G_{12} = G_{13} = G_{23} = 5.5 \text{ GPa},$$

$$\rho = 1580 \text{ kg/m}^3$$

Two cases of impact events are considered here, i.e., impact by a 7.5g mass with a velocity of 3m/s and by a 19.6g mass with a velocity of 10m/s, respectively. In the present study, the contact law defined in Eq.12a is simply employed for the whole contact processing. Since the laminate is thin one numerical layer is used with shear correction factor $k_{55}^2 = 0.88075$ and $k_{44}^2 = 0.73173$, evaluated by the method in Reference [26]

Case 1 Impact by a 7.5g mass of 3m/s

Numerical tests are carried out on the impact problem of the [0/90/0/90/0]_s laminated plate by a 7.5g mass with a velocity of 3m/s. The example chosen here is the one studied by Sun and Chen [37], and Qian and Swanson [28].

The convergence of time integration is first studied. Taking advantage of symmetry in this thin plate geometry, half of the plate (crosswise direction of the strip) is modelled using five quadratic strips in the crosswise direction. Each strip has ten sections in the longitudinal direction and one numerical layer through the thickness. The contact coefficient k_c is evaluated using Eq.13, which is equal to 25644 N/mm^{1.5}. The time increments are taken as 20 μs, 10 μs, 2 μs and 1 μs. Figs.4a and 4b show the contact force history and the central deflection of the plate, respectively. It can be seen that all the chosen time increments give stably converged solutions. As the time increment decreases, convergence behaviour can be observed. It is noted that the results for contact force and deflection histories obtained using a time increment of 20 μs are fairly reasonable. The results obtained by using a time increment of 2 μs are almost identical to those using a time increment of 1 μs, as well as 0.1 μs (not presented in the figure), within plotting accuracy. The predicted maximum contact forces are 303.2 N, 291.0 N, 290.2 N, and 290.4 N, respectively, when using time steps of 20μs, 10μs 2μs and 1μs, respectively.

Next, the convergence with respect to the plate mesh is investigated. Half of the plate is modelled using a number, n_e , of quadratic strips with different section number q as (1) $n_e=2, q=4$, (2) $n_e=3, q=6$, (3) $n_e=3, q=10$, (4) $n_e=5, q=10$, (5) $n_e=10, q=10$, and (6) $n_e=10, q=20$. The time increment is taken as $2 \mu\text{s}$. The contact coefficient k_c is equal to $25644 \text{ N/mm}^{1.5}$. Figs. 5a and 5b show the convergence of contact force and the central deflection histories with respect to the plate mesh. A converged trend can be observed in the figures as the number of the strip and sections increases. It is found that use of coarse mesh yields reasonable deflection prediction but unacceptable estimation of the contact force. Both the contact force and deflection histories calculated by using 5 strips with 10 sections are nearly as good as those using 10 strips with 20 sections.

The following set of numerical tests is carried out to study the effect of the contact coefficients. For the same impact problem, Sun and Chen [37] meshed one quarter of the plate with 8×8 nine-node quadrilateral finite elements and used a contact law as Eq.12 with $k_c = 44683 \text{ N/mm}^{1.5}$, whereas Qian [28] and Swanson applied the Rayleigh-Ritz technique (100×100 modes) and incorporated the contact law as Eq.12a with the contact area changing at each time step and $k_c = 26540 \text{ N/mm}^{1.5}$. In the present study, the contact law defined in Eq.12a is used with a series of contact coefficients, $k_c = 44683 \text{ N/mm}^{1.5}$ (the same as Sun and Chen for the loading processing), $k_c = 36266 \text{ N/mm}^{1.5}$ and $k_c = 25644 \text{ N/mm}^{1.5}$ (evaluated from Eq.13). Fig.6 shows the comparison of the contact force and central deflection histories. In the present FSM analysis, 20 quadratic strips with 40 sections are used to mesh the whole plate and the time increment is taken as $1 \mu\text{s}$. The predicted maximum contact forces are 303.8 N, 297.0 N, and 287.0 N, respectively, when using contact coefficients of $44638 \text{ N/mm}^{1.5}$, $36266 \text{ N/mm}^{1.5}$ and $25644 \text{ N/mm}^{1.5}$, respectively. It is noted that the contact force and deflection histories predicted by the present FSM using contact coefficient of $25644 \text{ N/mm}^{1.5}$ (close to that of Qian and Swanson) are basically the same as those of Qian and Swanson using the Rayleigh-Ritz method. Use of contact coefficients $44638 \text{ N/mm}^{1.5}$, the same value as used by Sun and Chen, gives an agreed prediction for the deflection history to that of Sun and Chen, but a slightly higher maximum contact force than that of Sun and Chen. Since spline functions are the smoothest piecewise polynomials, they possess the blended advantages of smooth analytical functions and versatile polynomials. As fewer degrees of freedom are required for the same accuracy, the present FSM is much more computationally efficient in comparison with the conventional FEM in which conventional polynomials are used. More details can be found in authors' earlier work [52, 54, 55].

Case 2 Impact by a 19.6g mass of 10m/s

Consider the [0/90/0/90/0]_s laminated plate impacted by a 19.6g mass with a velocity of 10m/s. In the present study, the contact coefficient is taken as $k_c = 4.468 \times 10^4 \text{ N/mm}^{1.5}$, the same value as that used by Chen and Sun [38] for loading process.

The convergence of the contact force and central deflection histories with respect to plate mesh is shown in Fig.7. The results are obtained using time step of 2 μs and quadratic strips with the meshes (1) ne=5, q=10, (2) ne=5, q=20, (3) ne=10, q=20, and (4) ne=10,q=40. It can be observed that all the meshes give a close prediction in the central deflection history and the maximum contact force. However, stable results for the contact force history are only achieved by using 10 quadratic strips with 20 sections at least. Note that in the case 1 example the use of 5 quadratic strips and 10 sections gives stable and good results for the contact force history. This indicates that the convergence behaviour is affected by the interaction of the plate and the impactor.

The previous analysis is performed using the defaulted type of simply supported boundary conditions as described at the beginning of this section, i.e., the in-plane movement of the sides is constrained in the tangent direction but allowed in the normal direction. Besides the defaulted one, another type is also considered of simply supported boundary conditions in which all the in-plane movement of the sides is constrained. In this analysis half of the plate is meshed into 10 quadratic strips with 40 sections. Fig.8 shows comparison between the results for the contact force and plate deflection obtained from use of the two types of simply supported boundary conditions as well as the linear analysis. In the figure, the defaulted type of simply supported boundary conditions is denoted as BC0 whilst the other one is denoted as BC1. The figure also gives the results for the same impact problem obtained from non-linear FEM analysis by Chen and Sun [38] and from a commercial FEM package, LS-DYNA3D, by Liu and Dang [16]. Chen and Sun obtained their results by meshing a quarter of the plate with 8x8 nine-node quadrilateral finite elements and used the contact law as given in Eq.12, whereas Liu and Dang performed their analysis using a 40 by 40 mesh. The boundary conditions of BC1 were used by all of them. In Fig.8 it is shown that when using the same boundary conditions the present results compare well with those obtained from the FEM analysis [38] and the LS-DYNA3D analysis [16]. For the contact force history, a very close agreement is found in Fig.8a between the present non-linear FSM analyses with two different type boundary conditions and linear FSM analysis. It is not strange, since the plate deflections are less than half of the plate thickness during the contact processing as shown in Fig.8b, and therefore, the geometrical non-linearity has a quite insignificant effect. However, it is clearly shown in Fig.8b

that predicted plate deflection responses from the present non-linear FSM analyses with use of BC0 and BC1 and linear FSM analysis are different from one another.

5.2 Quasi-isotropic plate subjected to drop-weight impact

Here consider the example of a steel drop-weight impact on a $[45/0/-45/90]_s$ quasi-isotropic plate of AS4/3502 graphite-epoxy which was studied by Ambur et al [31]. The dimensions of the experimental specimens were 254 mm long and 127 mm wide and the thickness of a single layer was 0.127 mm. The specimens were simply supported on all four edges and impacted on the plate centre at impact-damage-initiation threshold energy level of 0.6779J (6 in.-lb). The material properties of AS4/3502 are given as

$$E_1 = 137.8 \text{ GPa}, E_2 = 9.0 \text{ GPa}, \nu_{12} = 0.3,$$

$$G_{12} = G_{13} = 6.0 \text{ GPa}, G_{23} = 3.5 \text{ GPa},$$

$$\rho = 1570 \text{ kg/m}^3$$

In the present investigation, the plate model is used with the dimensions 241.3 mm long by 114.3 mm wide in view of the fact that the supports are located in from the actual specimen boundaries [32]. The whole plate is modelled using 20 quadratic strips with 40 sections and through the plate thickness one numerical layer is used since the laminate is quite thin. The mass of the impactor is taken as 1.18 kg, whilst two different values, 25.4 mm and 12.7 mm, of impact-tip diameters are considered for comparison. The calculations are performed using a time step of 0.1 ms and the contact coefficient evaluated from Eq.13. The results of contact force are shown in Fig.9a compared with the experimental data and the central deflection of the plate in Fig.9b. It can be found that the geometrically non-linear and linear analyses give marked different predictions for the impact response including contact force history, plate deflection and contact duration. The contact force predicted by the present geometrically non-linear analysis is closely compared with those from experiment whilst the linear analysis gives a poor prediction of the contact force. This indicates that geometric non-linearity has significant effects on the impact response and it has to be included in the analysis. It is observed that use of different impact tip diameters in the present calculation results in only slightly different prediction for the contact response. In other words, the total contact force and the plate deflection are insensitive to contact coefficient. The smaller maximum contact force corresponds to the bigger diameter of impact tip but however, this may be untrue for impact events other than the present specific case.

In an effort to understand the effect of the impact mass and velocity, analysis is also performed using an impact mass of 0.59 kg with a 12.7-mm-diameter impact tip but the impact energy is still 0.6779J. Using different time scales the results are compared with those obtained previously for an impact mass 1.18 kg of 12.7-mm-diameter impact tip in Fig.10. In the figure, the time scale for 1.18 kg mass is a unit whilst the time scale for 0.59 kg mass is equal to the ratio of momenta for 1.18 kg mass and 0.59 kg, i.e., $\sqrt{2}$. It is shown that during the impact contact period the results, both contact force and plate central-deflection, corresponding to those two masses are in a close agreement when using the time scales mentioned. This indicates that for a specified drop-weight impact event, the maximum contact force and the maximum plate deflection at the impact position depend on impact energy level but the contact period is dominated by the impact mass and a longer contact period arises from a bigger impact mass.

6 Concluding remarks

A Layerwise B-spline FSM has been developed for analysing the geometrically non-linear transient response of laminated composite plates to transverse low-velocity impact. To simplify the complicated contact analysis, a Hertz-type contact law has been incorporated into the finite strip model for accounting for the contact behaviour. The solution of the non-linear impact problem is sought using Newmark time integration scheme in conjunction with Newton-Raphson iteration. The geometrically linear transient analysis of the impact problem has been discussed briefly as well. With the neglect of impact-related terms, the developed procedure is capable of analysing plate transients under dynamic loading.

The capability of the model has been used in a few applications including the impact response analysis of a plate subjected to relatively-high and low-velocity impact. It should be noted that the impact energy in both cases are low to avoid material damage and delamination which are not dealt in the present work. It has been indicated that the convergence behaviour of the impact dynamic problem is affected by the interaction of the plate and the impactor. Comparison of the results obtained from the geometrically non-linear analysis has been made with those of small-deflection solution and/or available results gained from finite element calculation and experiment. This comparison demonstrates the validity of the analysis procedure as well as the effect of geometric non-linearity on plate response and contact force. The results show that for a specified drop-weight

impact event, the impact energy level dominates the maximum contact force and the maximum plate deflection at the impact position but the impact mass dominates the impact contact duration.

References

1. Abrate S. Impact on laminated composite materials. *Appl Mech Rev* 1991; 44(4):155-190.
2. Caprino G, Crivelli Visconti I, Di Ilio A. Elastic behaviour of composite structures under low velocity impact. *Composites* 1984; 15(3): 231-234.
3. Rotem A. Residual flexural strength of FRP composite specimens subjected to transverse impact loading. *SAMPE Journal* 1988; 24(2): 19-25.
4. Alderson KL, Evans KE. Dynamic analysis of filament wound pipe undergoing low velocity impact. *Composite Science and Technology* 1992; 45: 17-22.
5. Mili F, Necib B. Impact behavior of cross-ply laminated composite plates under low velocities. *Composite Structures* 2001; 51: 237-244.
6. Shivakumar KN, Elber W, Illg W. Prediction of low-velocity impact damage in thin circular laminates. *AIAA Journal* 1985; 23(3): 442-447.
7. Bucinell RB, Nuismer RJ, Koury JL. Response of composite plates to quasi-static impact events. In: O'Brien TK. *ASTM STP 1110*, 1991, p528-549.
8. Sjoblom PO, Hartness JT, Cordell TM, On low-velocity impact testing of composite materials. *Journal of Composite Materials* 1988; 22:30-52.
9. Toh SL, Gong SW, Shim VPW. Transient stresses generated by low velocity impact on orthotropic laminated cylindrical shells. *Composite Structures* 1995; 31: 213-228.
10. Gong SW, Shim VPW, Toh SL. Central and noncentral normal impact on orthotropic composite cylindrical shells. *AIAA Journal* 1996; 34(8): 1619-1626.
11. Gong SW, Lam KY. Effects of structural damping and stiffness on impact response of layered structure. *AIAA Journal* 2000; 38(9): 1730-1735.
12. Robinson P, Davies GAO. Impactor mass and specimen geometry effects in low velocity impact of laminated composites. *Int. J. Impact Eng.* 1992; 12(2): 189-207.

13. Collombet F, Bonini J, Lataillade JL. A three-dimensional modelling of low velocity impact damage in composite laminates. *Int. J. Numer. Meth. Engng.* 1996; 39: 1491-1516.
14. Bonini J, Collombet F, Lataillade JL. Numerical modelling of contact for low velocity impact damage in composite laminates. In: Aliabadi MH, Brebbia CA. *Contact Mechanics, 1st International Conference on Contact Mechanics*, Southampton, July 1993, p453-461.
15. Banerjee R. Numerical simulation of impact damage in composite laminates. *Proceedings of the American Society for Composites* 1992; p539-552.
16. Liu D, Dang X. Testing and simulation of laminated composites subjected to impact loading. In: Bucinell RB. *Composite Materials: Fatigue and Fracture, 7th Volume, ASTM STP 1330*, American Society for Testing and Materials, 1998, p173-184.
17. Luo RK, Green ER, Morrison CJ. Impact damage analysis of composite plates. *International Journal of Impact Engineering* 1999; 22: 435-447.
18. Green ER, Morrison CJ, Luo RK. Simulation and experimental investigation of impact damage in composite plates with holes. *Journal of Composite Materials* 2000; 34(6): 502-521.
19. Goo NS, Kim SJ. Dynamic contact analysis of laminated composite plates under low-velocity impact. *AIAA Journal* 1997; 35(9): 1518-1521.
20. Yang SH, Sun CT. Indentation law for composite laminates. *Composite Materials: Testing and Design (6th Conference)*, ASTM STP 787, 1982, p425-449.
21. Tan TM, Sun CT, Use of static indentation laws in the impact analysis of laminated composite plates. *Journal of Applied Mechanics* 1985; 52: 6-12.
22. Lesser AJ, Filippov AG. Kinetics of damage mechanics in laminated composites. *Int. SAMPE Symp. And Exhibition* 1991; 36 (Pt.1): 886-900.
23. Srinivasan K, Jackson WC, Hinkley JA. Response of composite materials to low velocity impact. *Int. SAMPE Symp. And Exhibition* 1991; 36 (Pt.2): 850-862.
24. Wu E, Shyu K. Response of composite laminates to contact loads and relationship to low-velocity impact. *Journal of Composite Materials* 1993; 27(15): 1443-1464.
25. Sun CT, Chattopadhyay S. Dynamic response of anisotropic laminated plates under initial stress to impact of a mass. *Journal of Applied Mechanics* 1975; 42: 693-698.
26. Whitney JM, Pagano NJ. Shear deformation in heterogeneous anisotropic plates. *J. Appl. Mech.* 1970; 37: 1031-1036.
27. Dobyns AL. Analysis of simply-supported orthotropic plates subject to static and dynamic loads. *AIAA Journal* 1981;19(5): 642-650.

28. Qian Y, Swanson SR. A Comparison of Solution Techniques for Impact Response of Composite Plates. *Composite Structures* 1990; 14: 177-192.
29. Carvalho A, Soares CG. Dynamic response of rectangular plates of composite materials subjected to impact loads. *Composite Structures* 1996; 34: 55-63.
30. Pierson MO, Vaziri R. Analytical solution for low-velocity impact response of composite plate. *AIAA Journal* 1996; 34: 1633-1640.
31. Ambur DR, Starnes JHJr, Prasad CB. Low-speed impact damage-initiation characteristics of selected laminated composite plates. *AIAA Journal* 1995; 33: 1919-1925.
32. Ambur DR, Starnes JHJr, Prasad CB. Influence of impact parameters on the response of laminated composite plates. In: Martin RH. *Composite Materials: Fatigue and Fracture-Fifth Volume*, ASTM STP 1230, American Society for Testing and Materials, Philadelphia, 1995, p389-404.
33. Heitzer J. Dynamic interaction of a plate and an impactor. *Computers and Structures* 1996; 60(5): 837-848.
34. Wang H, Vu-Khanh T. Damage extension in carbon fiber/PEEK crossply laminates under low velocity impact. *J. Compos. Mater.* 1994; 28(8): 684-707.
35. Wang H, Vu-Khanh T. Fracture mechanics and mechanisms of impact-induced delamination in laminated composites. *J. Compos. Mater.* 1995; 29(2): 156-178.
36. Hu N, Sekine H, Fukunaga H, Yao ZH. Impact analysis of composite laminates with multiple delaminations. *International Journal of Impact Engineering* 1999; 22: 633-648.
37. Sun CT, Chen JK. On the Impact of Initially Stressed Composite Laminates. *Journal of Composite Materials* 1985; 19: 490-504.
38. Chen JK, Sun CT. Dynamic large deflection response of composite laminates subjected to impact. *Composite Structures* 1985; 4: 59-73.
39. Wu HT, Chang FK. Transient dynamic analysis of laminated composite plates subjected to transverse impact, *Computers and Structures* 1989; 31: 453-466.
40. Wu HT, Springer GS. Impact induced stresses, strains, and delaminations in composite plates. *Journal of Composite Materials* 1988; 22: 533-560.
41. Choi HY, Chang FK. A model for predicting damage in graphite/epoxy laminated composites resulting from low-velocity point impact. *J. Compos. Mater.* 1992; 26(14): 2134-2169.
42. Finn SR, He YF, Springer GS. Delaminations in composite plates under transverse static or impact loads – A method. *Composite Structures* 1993; 23: 177-190.
43. Finn SR, He YF, Springer GS. Delaminations in composite plates under transverse static or impact loads – Experimental results. *Composite Structures* 1993; 23: 191-204.

44. Scarponi C, Briotti G, Barboni R. Impact testing on composite laminates and sandwich panels. *Journal of Composite Materials* 1996; 30(17): 1873-1911.
45. Choi HY, Downs RJ, Chang FK. A new approach toward understanding damage mechanisms and mechanics of laminated composites due to low-velocity impact: part I – experiments. *J. Compos. Mater.* 1991; 25: 992-1011.
46. Choi HY, Wu HYT, Chang FK. A new approach toward understanding damage mechanisms and mechanics of laminated composites due to low-velocity impact: part II – analysis. *J. Compos. Mater.* 1991; 25: 1012-1038.
47. Choi HY, Wang HS, Chang FK. Effect of laminate configuration and impactor's mass on initial impact damage of composite plates due to line-loading impact. *J. Compos. Mater.* 1992; 26(6): 804-827.
48. Davies GAO, Zhang X, Zhou G, Watson S. Numerical modelling of impact damage. *Composites* 1994; 25(5): 342-350.
49. Davies GAO, Zhang X. Impact damage prediction in carbon composite structures. *Int. J. Impact Engng.* 1995; 16: 149-170.
50. Zhang X. Impact damage in composite aircraft structures – experimental testing and numerical simulation. *Proc. Instn. Mech. Engrs.* 1998; 212(part G): 245-259.
51. Wiggendaad JFM, Zhang X, Davies GAO. Impact damage prediction and failure analysis of heavily loaded, blade-stiffened composite wing panels. *Composite Structures* 1999; 45: 81-103.
52. Zhang Y, Wang S, Petersson B. Large deflection analysis of composite laminates. *Journal of Materials Processing Technology* 2003; 138: 34-40.
53. Reddy JN. A Generalization of Two-dimensional Theories of Laminated Composite Plates. *Communications in Applied Numerical Methods* 1987; 3: 173-180.
54. Wang S, Chen J, Dawe DJ. Linear transient analysis of rectangular laminates using spline finite strips. *Composite Structures* 1998; 41(1): 57-66.
55. Chen J, Dawe DJ, Wang S. Nonlinear transient analysis of rectangular composite laminated plates. *Composite Structures* 2000; 49(2): 129-139.
56. Belytschko T, Schoebele DF. On the unconditional stability of an implicit algorithm for non-linear structural dynamics. *ASME Journal of Applied Mechanics* 1975; 17: 865-869.

Figure legend

Fig. 1 Transverse impact on a rectangular plate

Fig. 2 In-plane displacement configuration of layerwise theory

Fig. 3 A typical layerwise finite strip element

Fig. 4 Convergence with respect to time step for the problem of a $[0/90/0/90/0]_s$ plate impacted by a 7.5g mass of 3m/s

Fig. 5 Convergence with respect to plate mesh for the problem of a $[0/90/0/90/0]_s$ plate impacted by a 7.5g mass of 3m/s

Fig. 6 Comparison of predicted contact force and central deflection histories of a $[0/90/0/90/0]_s$ plate impacted by a 7.5g mass of velocity 3m/s

Fig. 7 Convergence with respect to plate mesh for the problem of a $[0/90/0/90/0]_s$ plate impacted by a 19.6 g mass of velocity 10 m/s

Fig. 8 Comparison of predicted central deflection history of a $[0/90/0/90/0]_s$ plate impacted by a 19.6 g mass of velocity 10 m/s

Fig. 9 Comparison of impact response of a $[45/0/-45/90]_s$ plate to drop-weight

Fig. 10 Comparison of impact response of a $[45/0/-45/90]_s$ plate to masses 1.18kg and 0.59kg at a given impact energy of 0.6779J

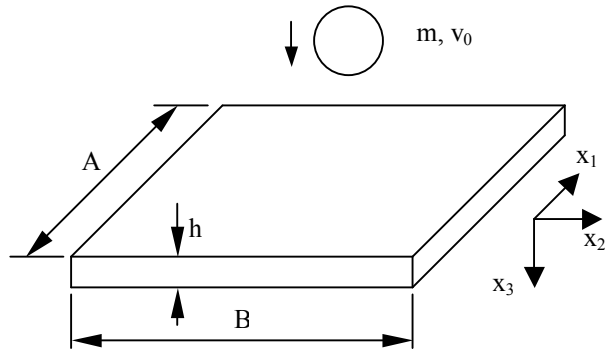


Fig. 1 Transverse impact on a rectangular plate

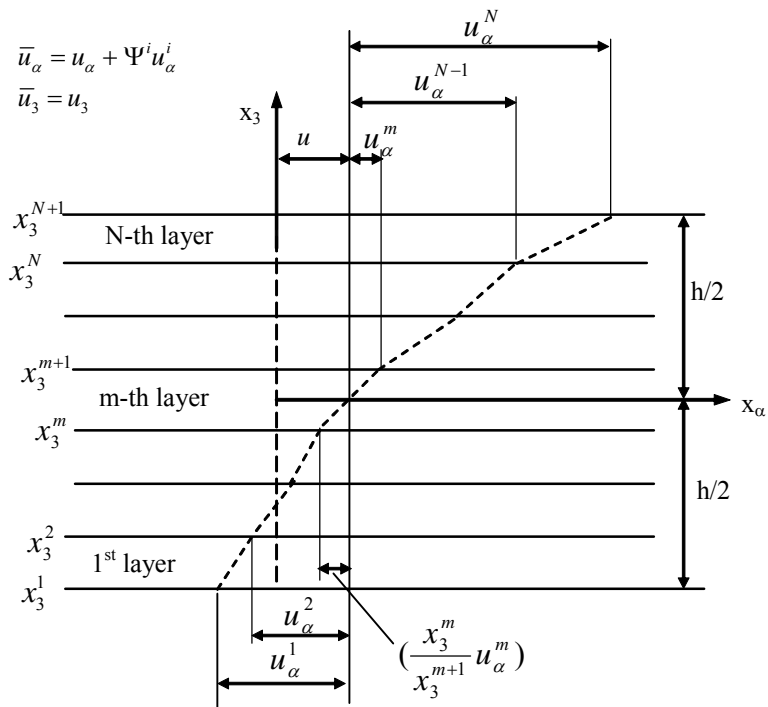


Fig. 2 In-plane displacement configuration of layerwise theory

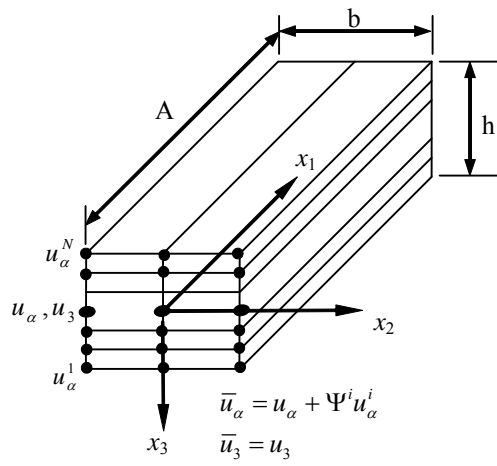
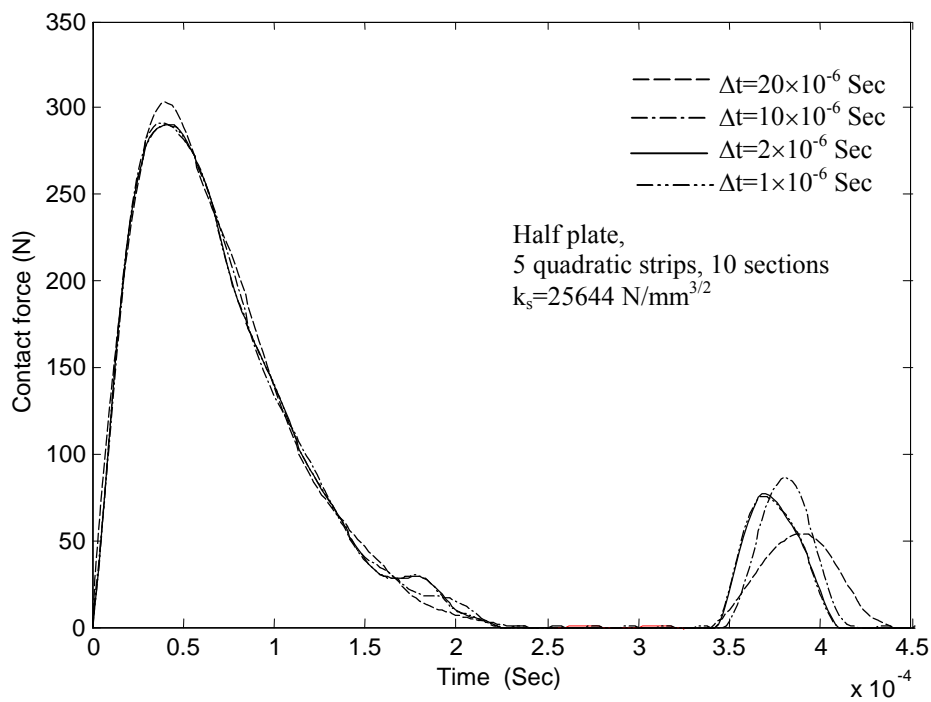
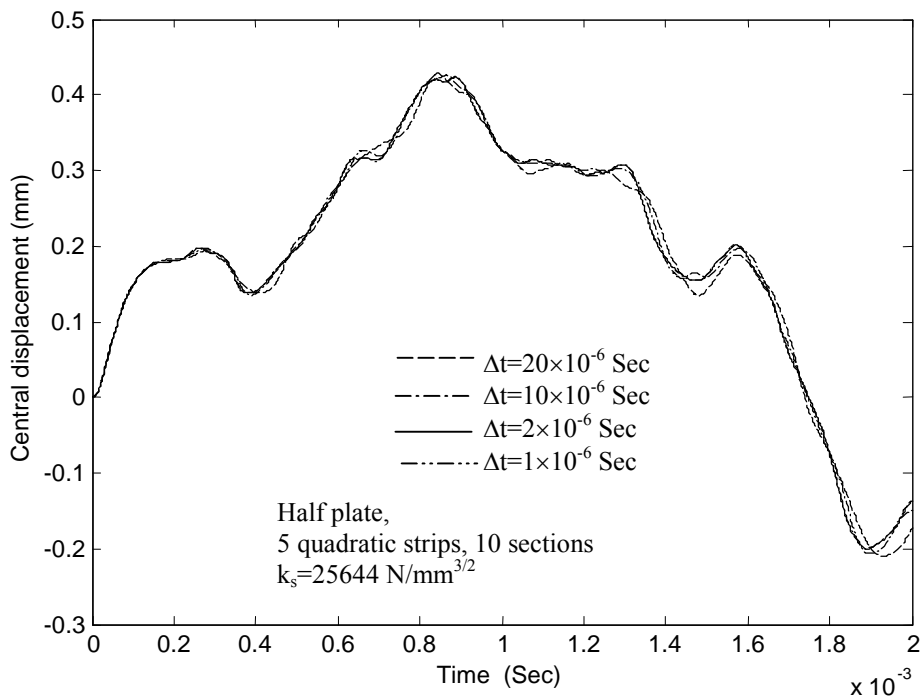


Fig. 3 A typical layerwise finite strip element

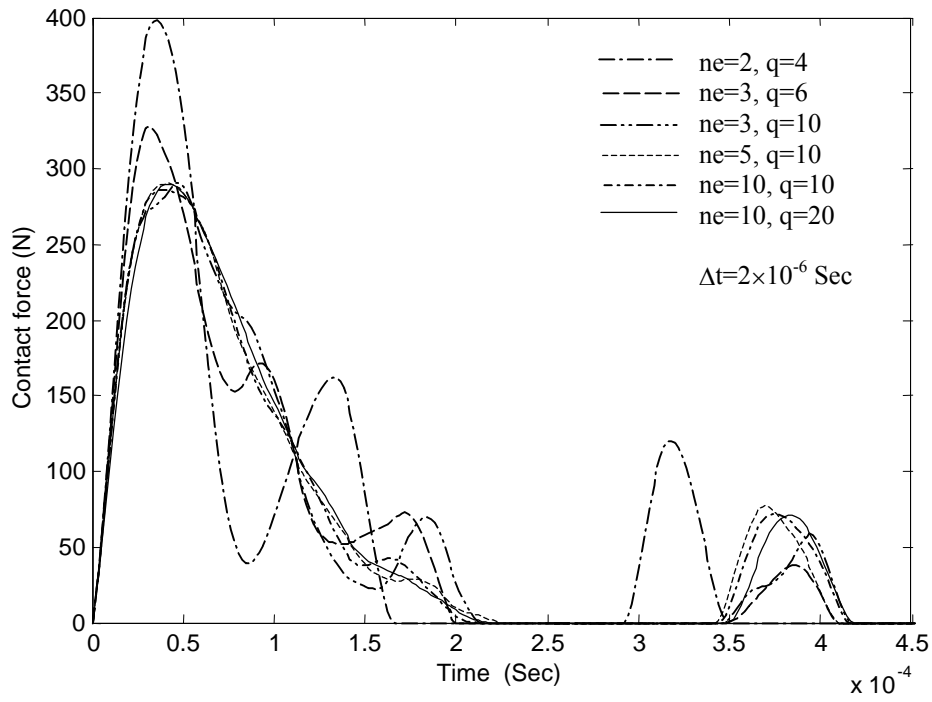


(a) Contact force

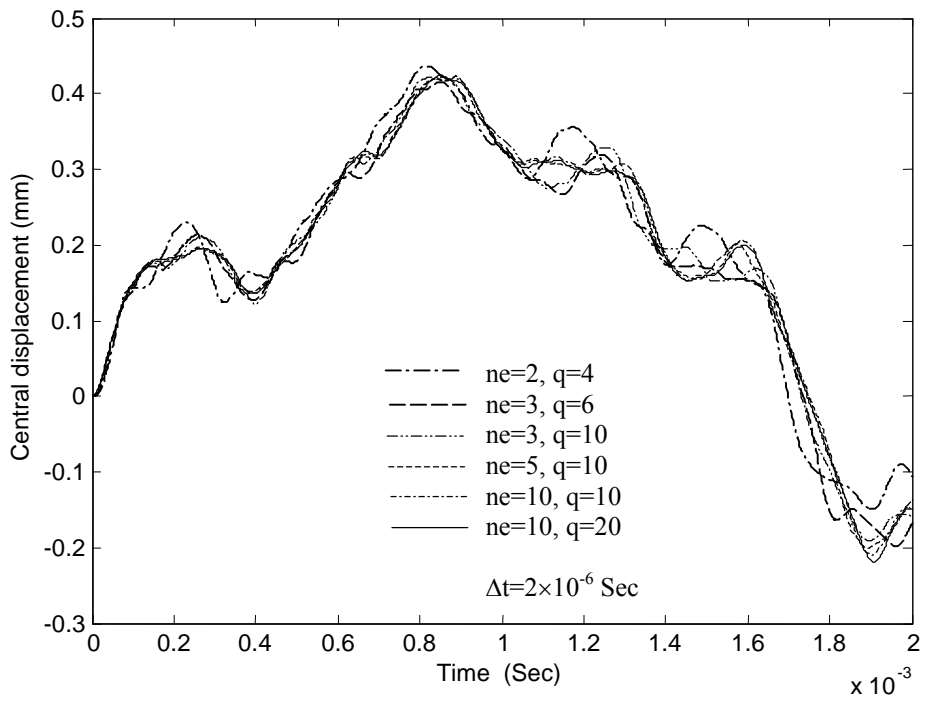


(b) Central deflection

Fig. 4 Convergence with respect to time step for the problem of a $[0/90/0/90/0]_s$ plate impacted by a 7.5g mass of 3m/s

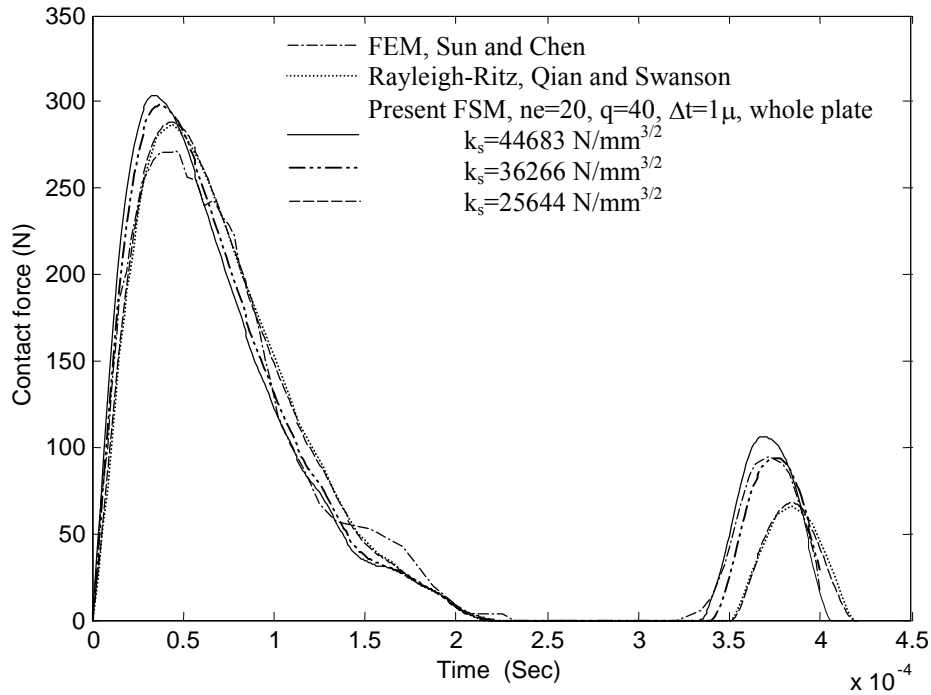


(a) Contact force

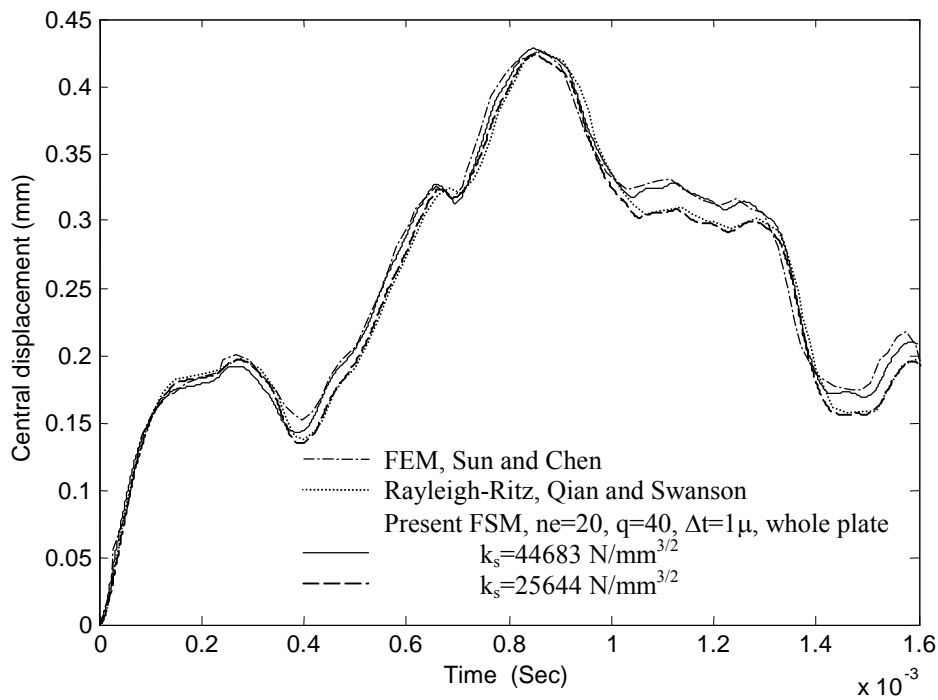


(b) Central deflection

Fig. 5 Convergence with respect to plate mesh for the problem of a $[0/90/0/90/0]_s$ plate impacted by a 7.5g mass of 3m/s

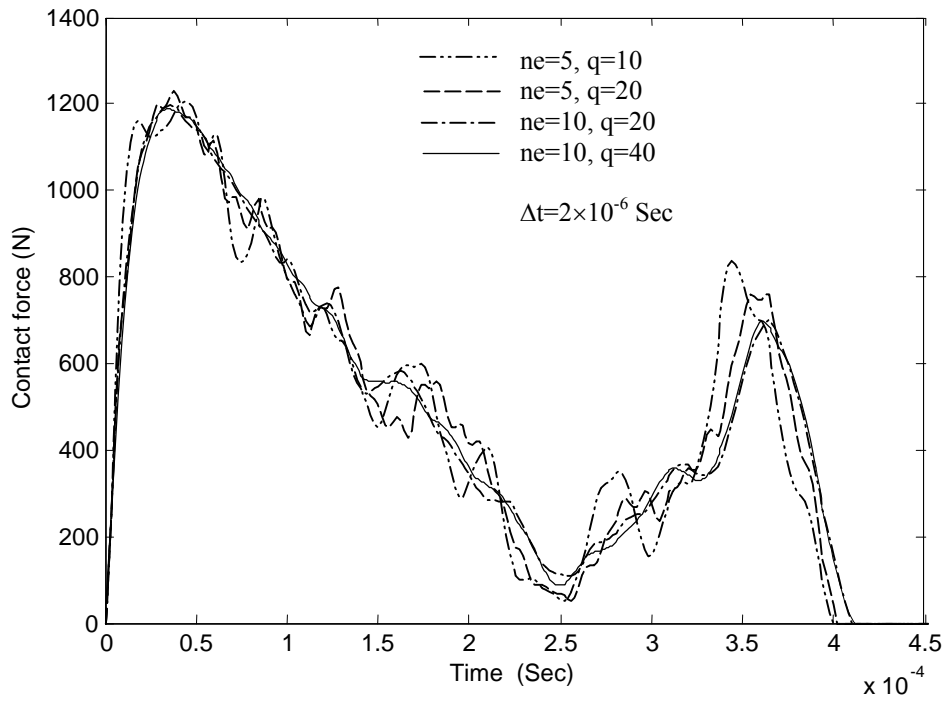


(a) Contact force

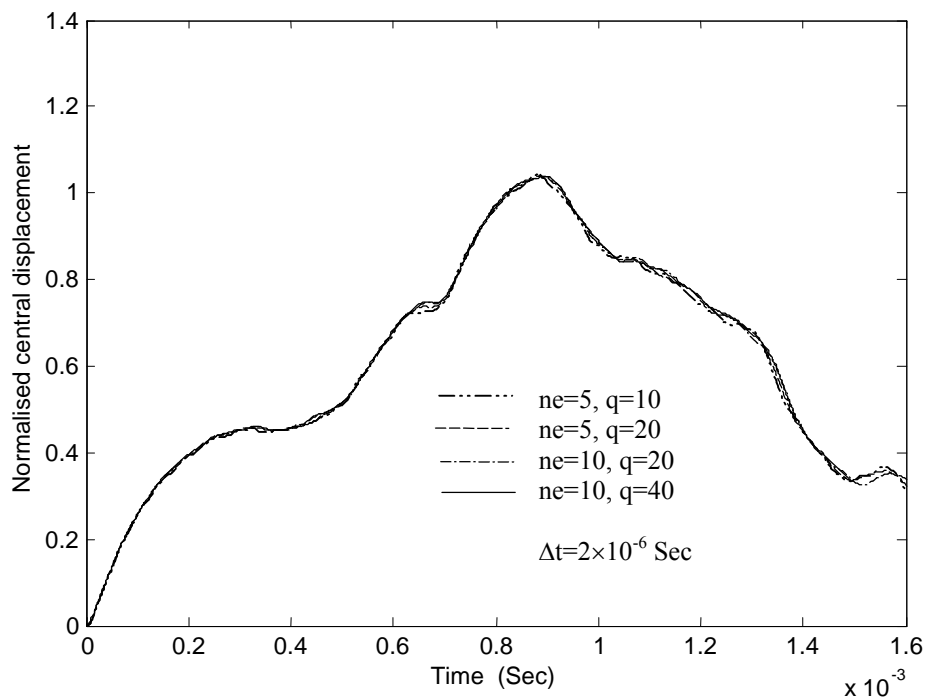


(b) Central deflection

Fig. 6 Comparison of predicted contact force and central deflection histories of a $[0/90/0/90/0]_s$ plate impacted by a 7.5g mass of velocity 3m/s

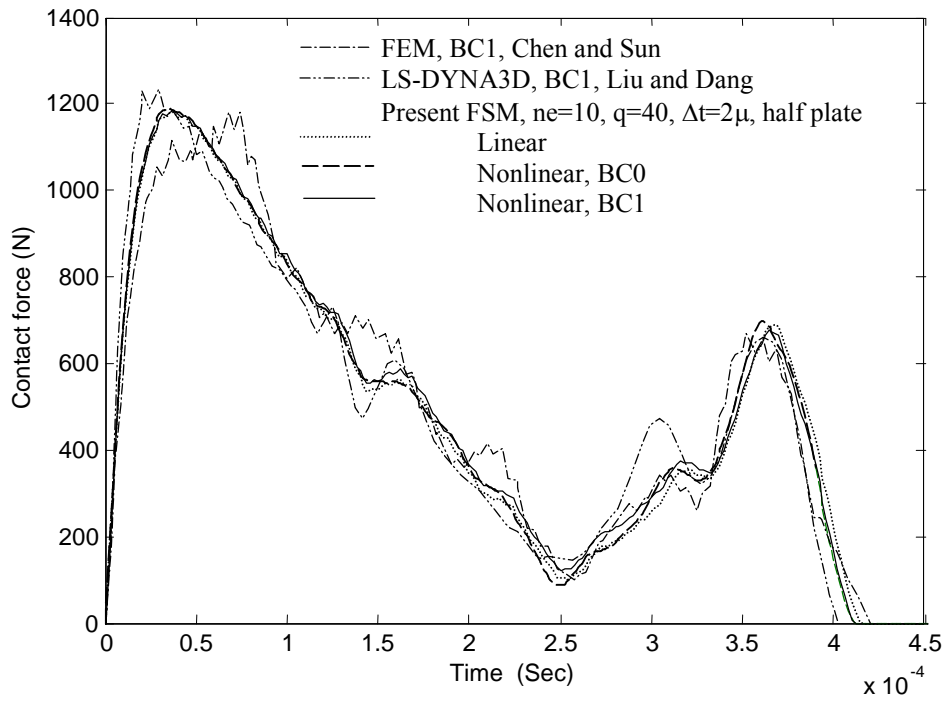


(a) Contact force

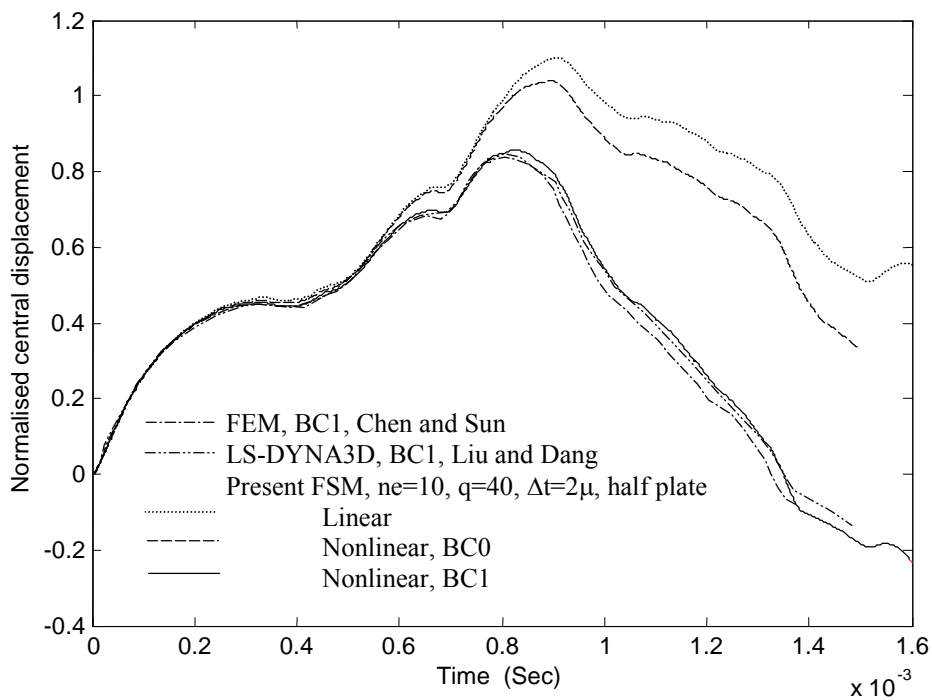


(b) Central deflection

Fig. 7 Convergence with respect to plate mesh for the problem of a $[0/90/0/90/0]_s$ plate impacted by a 19.6 g mass of velocity 10 m/s

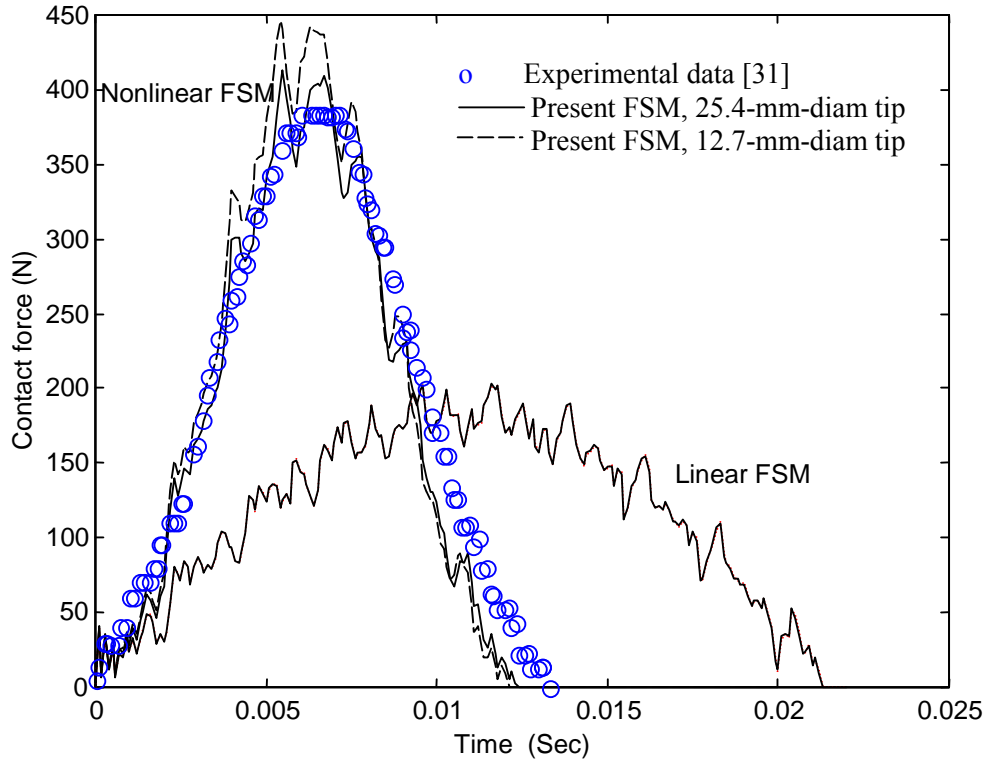


(a) Contact force

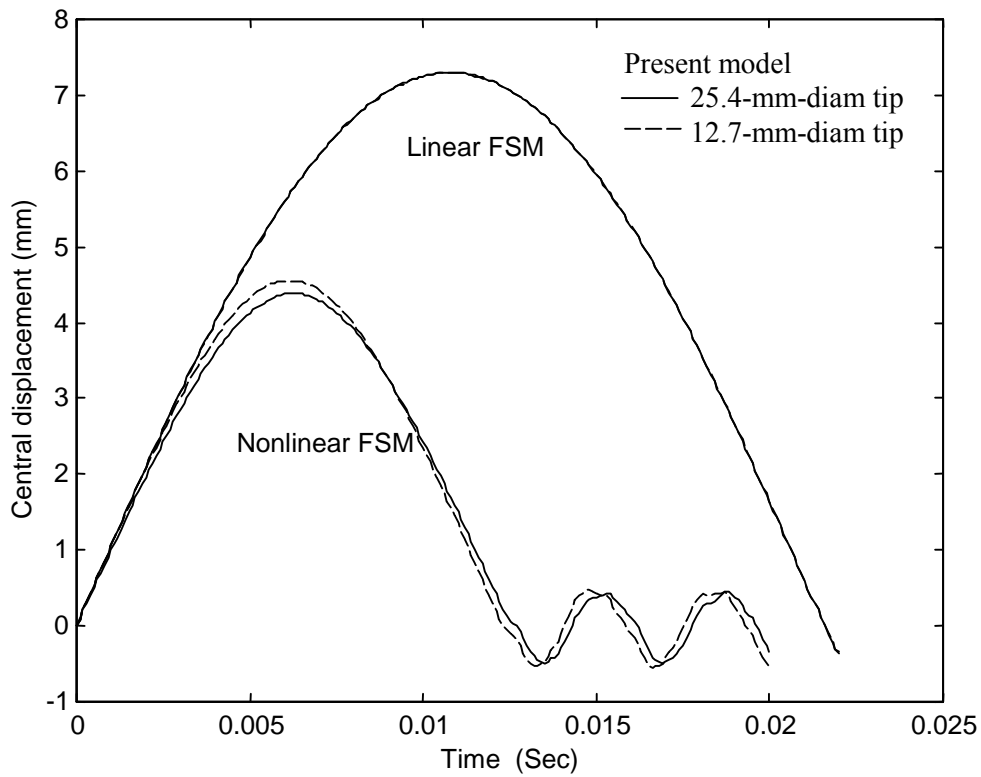


(b) Central deflection

Fig. 8 Comparison of predicted central deflection history of a $[0/90/0/90/0]_s$ plate impacted by a 19.6 g mass of velocity 10 m/s



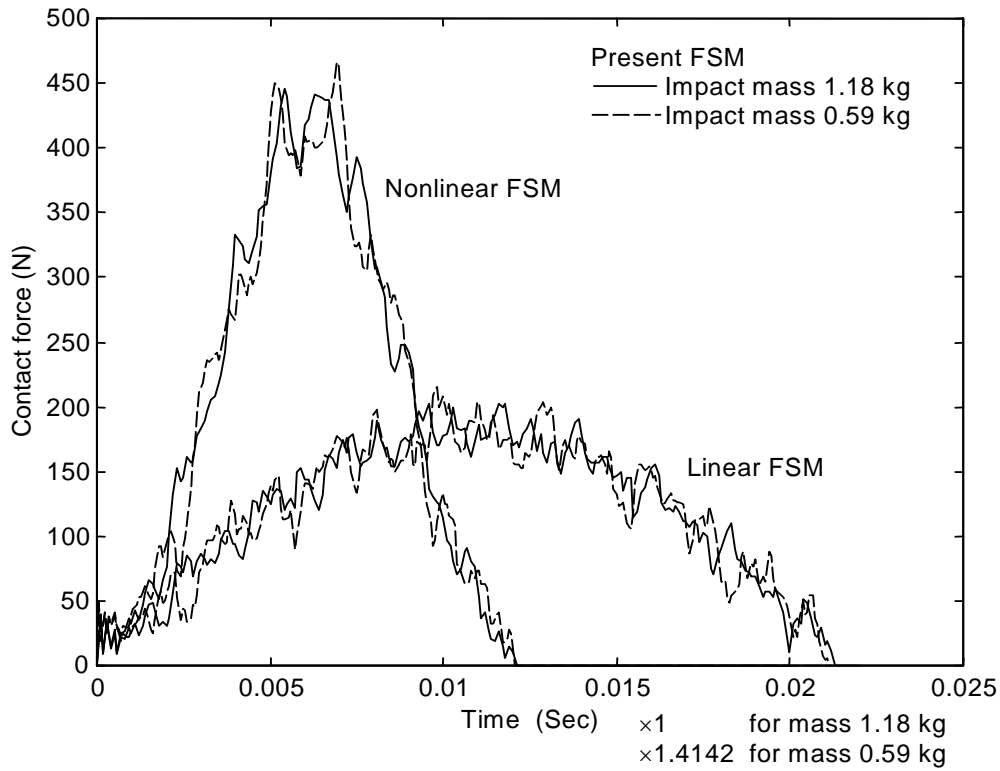
(a) Contact force history



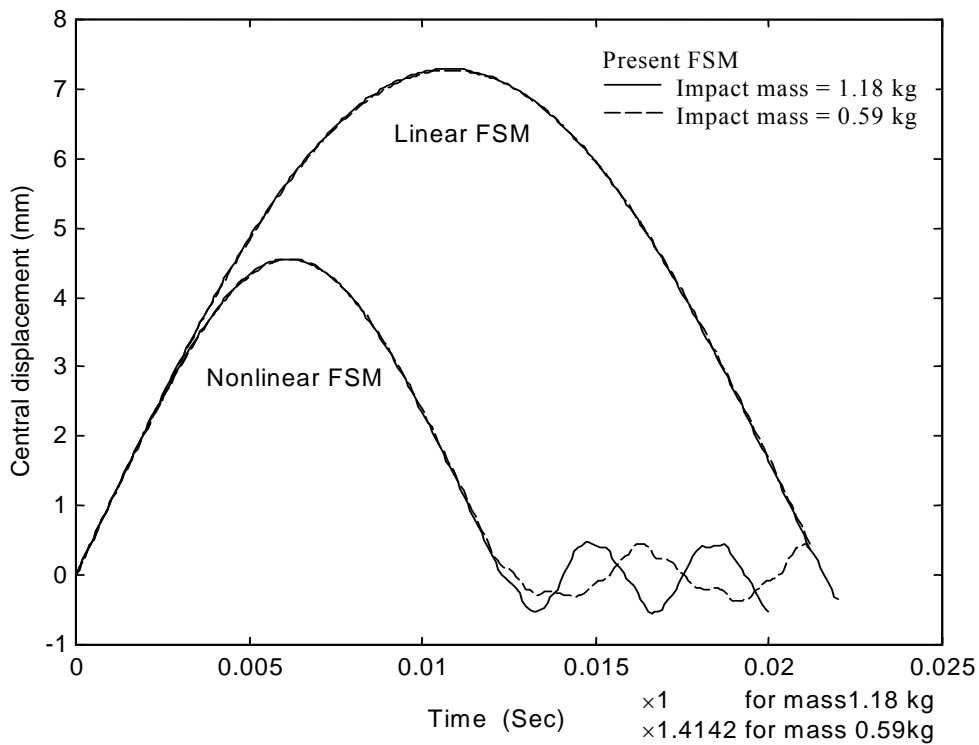
(b)

Central deflection of the plate

Fig. 9 Comparison of impact response of a $[45/0/-45/90]_s$ plate to drop-weight



(a) Contact force history



(b) Central deflection of the plate

Fig. 10 Comparison of impact response of a $[45/0/-45/90]_s$ plate to masses 1.18kg and 0.59kg at a given impact energy of 0.6779J